Stereochemical Origin of Opposite Orientations in DNA Adducts Derived from Enantiomeric *anti*-Benzo[a]pyrene Diol Epoxides with Different Tumorigenic Potentials†

Xiao-Ming Xie,‡ Nicholas E. Geacintov,‡ and Suse Broyde*,§

Chemistry and Biology Departments, New York University, New York, New York 10003

Received October 27, 1998

ABSTRACT: When covalently linked to DNA, enantiomeric pairs of mirror image aromatic diol epoxides with differing tumorigenic potencies adopt opposite orientations along the DNA helix. This phenomenon has been observed by high-resolution NMR solution studies in a number of systems. Preliminary modeling efforts [Geacintov et al. (1997) *Chem. Res. Toxicol. 10,* 111−146) had suggested that the origin of the opposite orientation effect may be manifested even at the level of the carcinogen-modified nucleoside due to primary steric hindrance effects between the aromatic moiety and the attached base and sugar. Such a small system can be computationally investigated extensively, since a very thorough survey of the potential energy surface is feasible. Consequently, in an effort to understand the underlying origins of the opposite orientations in (+)-*trans* and (−)-*trans-anti* adduct pairs, we have undertaken an extensive investigation of the paradigm 10*S* (+) and 10*R* (−)-*trans-anti*-[BP]-N^2-dG mononucleoside adduct pair, derived from the binding of the (+)-7*R*,8*S*,9*S*,10*R* and (−)-7*S*,8*R*,9*R*,10*S* enantiomers of 7,8-dihydro-9,-10-epoxy-7,8,9,10-tetrahydrobenzo[a]pyrene (BP) to the exocyclic amino group of 2′-deoxyguanosine. In the present work we created 373248 different conformers for each adduct, which uniformly sampled the possible rotamers about the three flexible torsion angles governing the orientation of the base (χ) and its covalently linked BP residue (α', β') at 5° intervals, and computed each of their energies with AMBER 4.0. The extensive results permitted us to map the potential energy surface of the molecule. Only four low-energy structural domains are found for the (+)-*trans* adduct and four for the (−)-*trans* adduct; the (+)/(−) pairs of each structural domain are mirror images, with the mirror image symmetry broken by the sugar and its attached C4′−C5′ group. The most favored of these four is observed experimentally in the duplexes containing the same (+) and (−)-*trans-anti*-[BP]-N^2-dG adducts (Cosman et al. (1992) *Proc. Natl. Acad. Sci. U.S.A. 89,* 1914−1918; de los Santos et al. (1992) *Biochemistry 31,* 5245−5252). The origin of the opposite orientations resides in steric hindrance effects resulting from the mirror image relationship of the BP benzylic rings in the adduct pair, such that rotation of one stereoisomer into the conformational domain preferred by the other causes crowding between the base and the BP benzylic ring. Limited conformational flexibility in the torsion angle β', the one closest to the bulky BP moiety at the linkage site to guanine, plays a key role in governing the orientations in each adduct. The opposite orientation phenomenon is likely to manifest itself when the adducts are processed by cellular enzymes involved in replication, repair, and transcription and thus play a role in the differing biological outcomes stemming from the (+) and (−)-*trans-anti* adducts.

Benzo[a]pyrene is a polycyclic aromatic hydrocarbon present widely in the environment, in automobile exhaust, in tobacco smoke, and as a contaminant in foods such as vegetable oils (*1*−*3*). It is metabolically activated to highly reactive diol epoxides (reviewed in ref *4*) which bind chemically to cellular DNA and cause mutations in oncogenes (*5*) and tumor suppressor genes (*6*) that can lead to cancers. Among the metabolic activation products of benzo[a]pyrene are a pair of mirror image diol epoxides, (+)-7*R*,8*S*-dihydroxy-9*S*,10*R*-epoxy-7,8,9,10-tetrahydrobenzo[a]-pyrene and the corresponding (−)-7*S*,8*R*,9*R*,10*S* enantiomer known as (+) and (−)-*anti*-benzo[a]pyrene diol epoxide (BPDE). These have long been of interest because the (+) enantiomer is highly tumorigenic in mice while the (−) enantiomer is not (*7, 8*). The (+) enantiomer is also more mutagenic than the (−) one in mammalian systems (*9*).

Both (+) and (−)-*anti*-BPDE react with DNA principally at the exocyclic amino group of guanine to form covalent adducts (*10, 11*). *Cis* and *trans* addition are possible in each case, leading to four adducts: 10*S* (+) and 10*R* (−)-*trans-anti* and 10*R* (+) and 10*S* (−)-*cis-anti*-[BP]-N^2-dG, where the 10*R* and 10*S* denote the absolute configuration at the C10 linkage site of BPDE. The present work focuses on the (+) and (−)-*trans-anti* adducts with 10*S* and 10*R* stereo-

† This research is supported by NIH Grants CA 28038 and RR-06458, and DOE Grant DE-FG02-90ER60931 to S. B., and NIH Grant CA-20851 to N.E.G.

* Corresponding author Phone: (212) 998-8231. Fax (212) 995-4015. E-mail: broyde@nyu.edu.

‡ Chemistry Department.

§ Biology Department.

10.1021/bi9825605 CCC: $18.00
Published on Web 02/20/1999

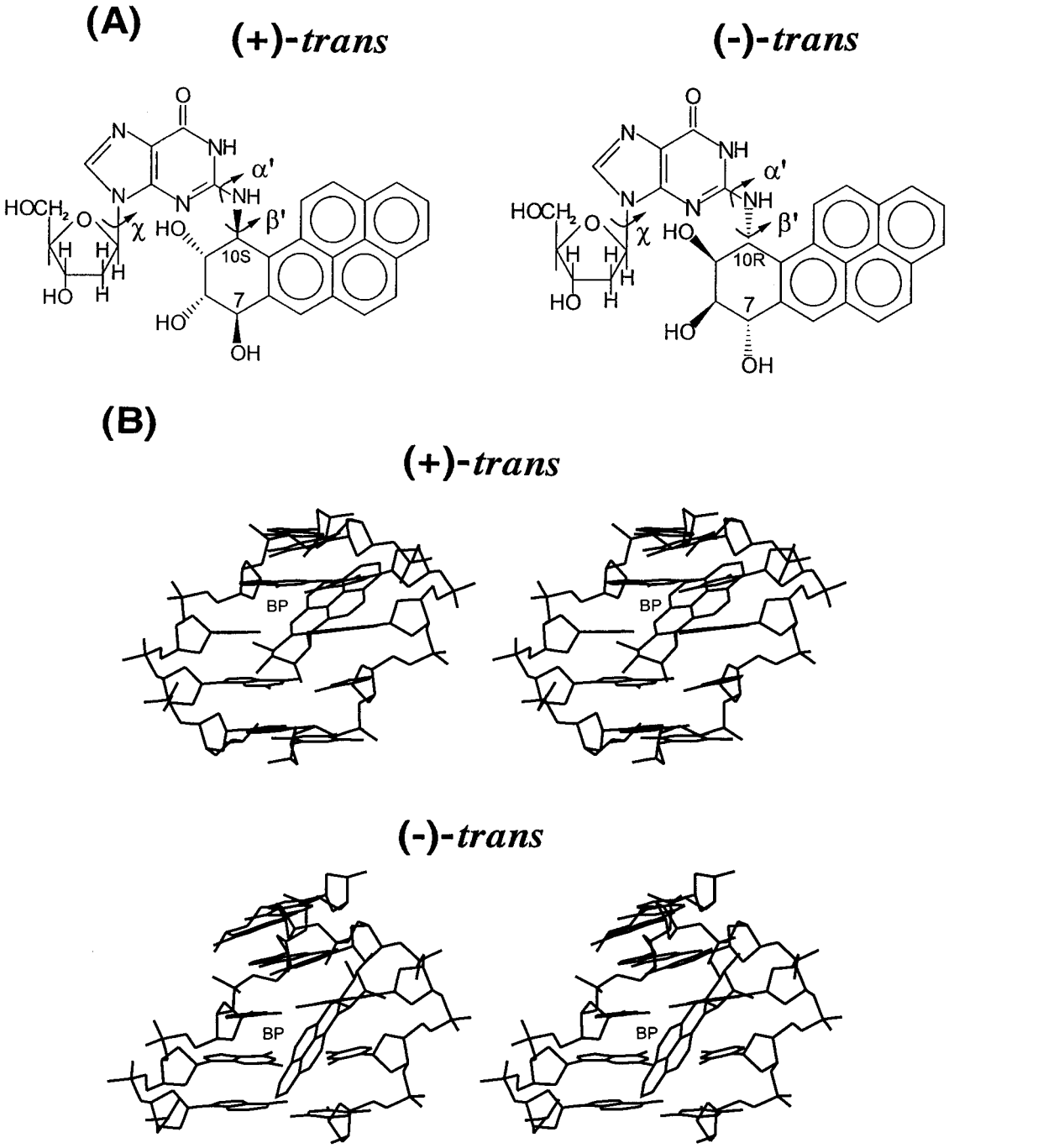

FIGURE 1: (A) Structures of (+) and (−)-*trans-anti*-[BP]-N^2-dG nucleoside adducts. Torsion angles χ, α', β' are defined as follows: χ, O4′-C1′-N9-C4; α', N1-C2-N^2-C10(BP); β', C2-N^2-C10(BP)-C9(BP). (B) NMR solution structures of (+) and (−)-*trans-anti*[BP]-N^2-dG adducts (*16*, *18*). Central modified duplex 5-mer of 11-mer is shown in stereo.

chemistry, respectively, at the linkage site to guanine (Figure 1).

Because of the striking differences in tumorigenicity of (+) and (−)-*anti* BPDE, the structures of their adducts with DNA have been of great interest. The 10*S* (+)-*trans-anti*-[BP]-N^2-dG adduct is the major reaction product of the tumorigenic (+)-*anti*-BPDE with native DNA (about 90%) (*11*−*14*) and is therefore considered to be of special importance. The analogous 10*R* (−)-*trans-anti*-[BP]-N^2-dG adduct is a significant component (about 63%) of the reaction of (−)-*anti*-BPDE with native DNA (*11*).

Computational studies for duplex DNA modified with these two lesions suggested that the BP moiety would take up opposite orientations along the DNA in (+) and (−)-*trans-anti*-[BP]-N^2-dG adducts (*15*). Independent high-resolution NMR studies in solution revealed experimentally that opposite orientations are indeed observed. In a normal duplex, the BP moiety in the (+)-*trans* adduct is situated in the B-DNA minor groove, directed 5′ along the modified strand (*16*, *17*); in the (−) adduct, the BP is directed 3′ along the modified strand in the minor groove (*18*). Furthermore, the opposite orientation phenomenon is also observed, but manifested differently in a "deletion" duplex, in which there are 11 residues on the modified strand and only 10 on the partner, with the BP-modified dG containing no partner residue (as if the replication machinery had skipped the BP

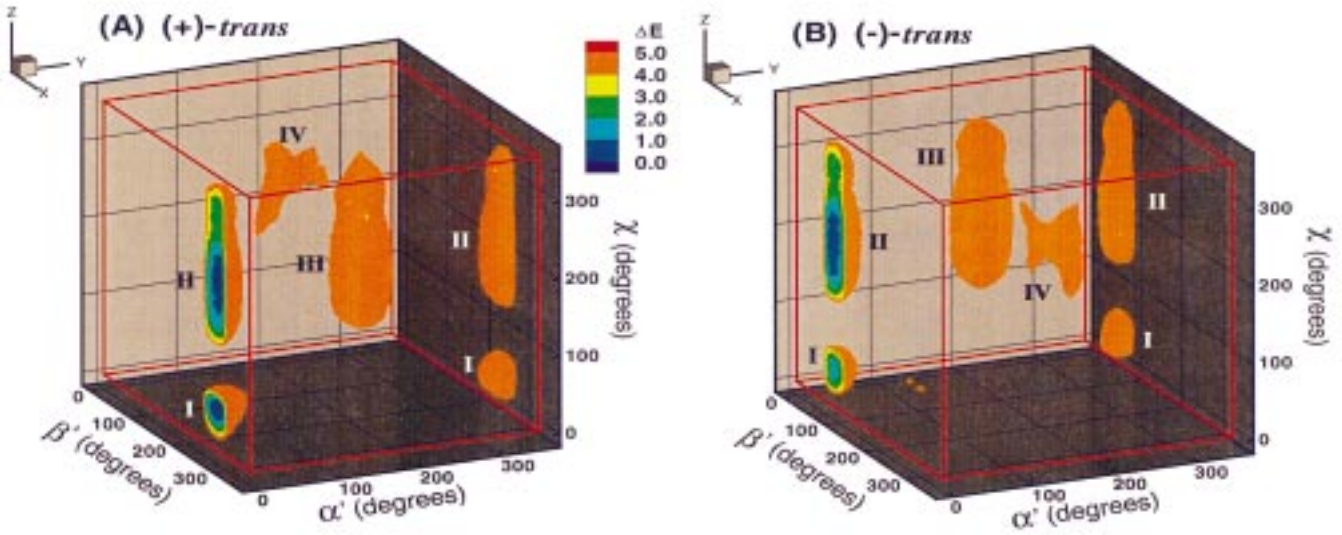

FIGURE 2: Three-dimensional χ, α', and β' energy topographies to 5 kcal/mol. I−IV denote the 4 low energy domains. Torsion angles cycle over 360°, so 359° is actually contiguous with 0°: A, (+)-*trans-anti*-[BP]-N^2-dG adduct; B, (−)-*trans-anti*-[BP]-N^2-dG adduct.

Table 1: Number of Conformers in 1 kcal/mol Shells in (+) and (−)-*trans-anti*-[BP]-N^2-dG Adducts, to 5 kcal/mol

	0−1 kcal/mol		1−2 kcal/mol		2−3 kcal/mol		3−4 kcal/mol		4−5 kcal/mol		total	
domain	(+)	(−)	(+)	(−)	(+)	(−)	(+)	(−)	(+)	(−)	(+)	(−)
I	80	0	144	30	276	195	351	307	404	350	1255	882
II	27	0	122	31	502	388	644	709	693	816	1988	1944
III	468	479	1651	1658	2034	1947	2080	1998	1967	1917	8200	7999
IV	0	47	49	129	129	214	222	278	343	340	743	1008
total	575	526	1966	1848	2941	2744	3297	3292	3407	3423	12186	11833

Table 2: Domains of Low-Energy Wells in (+) and (−)-*trans-anti*-[BP]-N^2-dG Adducts[a]

			β' domain (deg)	
domain	χ domain (deg)	α domain (deg)	(+) adduct	(−) adduct
I	45 ± 25 (*syn*)	0 ± 40	−90 ± 40	90 ± 40
II	210 ± 75 (*anti*)	0 ± 40	−90 ± 40	90 ± 40
III	210 ± 75 (*anti*)	180 ± 40	−90 ± 40	90 ± 40
IV	255 ± 35 (*anti*)	180 ± 40	105 ± 35	−110 ± 35

[a] Domains of the 5 kcal/mol surface were approximated to ±5°. χ and α' domains are the same for (+) and (−) adducts. For α' this is the case because 0° and 180° are the same as their sign inverted values. Because of the cycling of the torsion angles over 360°, −90° is the same as 270° and −110° is the same as 250°.

damaged residue). In this case, the BP is intercalated into the helix with displacement of the modified guanine in both (+) and (−) adducts, but in the (+) case this guanine and its attached BP benzylic ring reside on the *major* groove side of the helix cylinder (*19*), while in the (−) adduct the displaced guanine and attached benzylic ring are situated on the opposite, *minor* groove side of the helix cylinder (*20*).

The opposite orientation effect in adducts derived from enantiomeric (+) and (−) pairs of diol epoxide derivatives of aromatic hydrocarbons has been observed in a number of adduct pairs, as reviewed in Geacintov et al. (*21*) and Jerina et al. (*22*), irrespective of the specific conformation adopted by the aromatic moiety in relation to the DNA (in the minor groove (*16*−*18, 23*), in the major groove (*24, 25*), base displaced-intercalated (*19, 20, 26*−*28*), quasi-classically intercalated (*29*−*33*)), irrespective of the specific base modified (guanine or adenine), and irrespective of the specific aromatic moiety. Thus, this opposite orientation phenomenon appears to be a general one whose underlying stereochemical origins require elucidation.

Preliminary modeling efforts (*21*) have suggested that the origin of the opposite orientation effect may be manifested even at the level of the modified nucleoside due to primary steric hindrance effects between the aromatic moiety and the attached base and sugar groups. Such a small system can be computationally investigated extensively, since a very thorough survey of the potential energy surface is feasible. Consequently, in an effort to understand the underlying origins of the opposite orientations in the (+) and (−) adduct pairs and to elucidate inherent conformational flexibilities in this effect, we have undertaken an extensive investigation of the (+) and (−)-*trans-anti*-[BP]-N^2-dG mononucleoside adducts as these are considered a paradigm of the stereoisomeric properties of polynuclear aromatic diol-epoxide DNA adduct pairs.

In the present work we created 373248 different conformers for each adduct, which uniformly sampled the possible rotamers about three flexible torsion angles χ, α', and β' (Figure 1) at 5° intervals, and computed each of their energies. The extensive results permitted us to map the potential energy surface of the molecules. Only four potential energy wells or structural domains are found for the (+)-*trans* adduct and four for the (−)-*trans*. The (+)/(−) pairs of each structural domain are nearly mirror images, with the mirror image symmetry broken by the sugar and its attached C4′−C5′ group. The most favored of these domains is observed experimentally in the duplexes modified by each adduct (*16, 18*−*20*). The origin of the opposite orientations

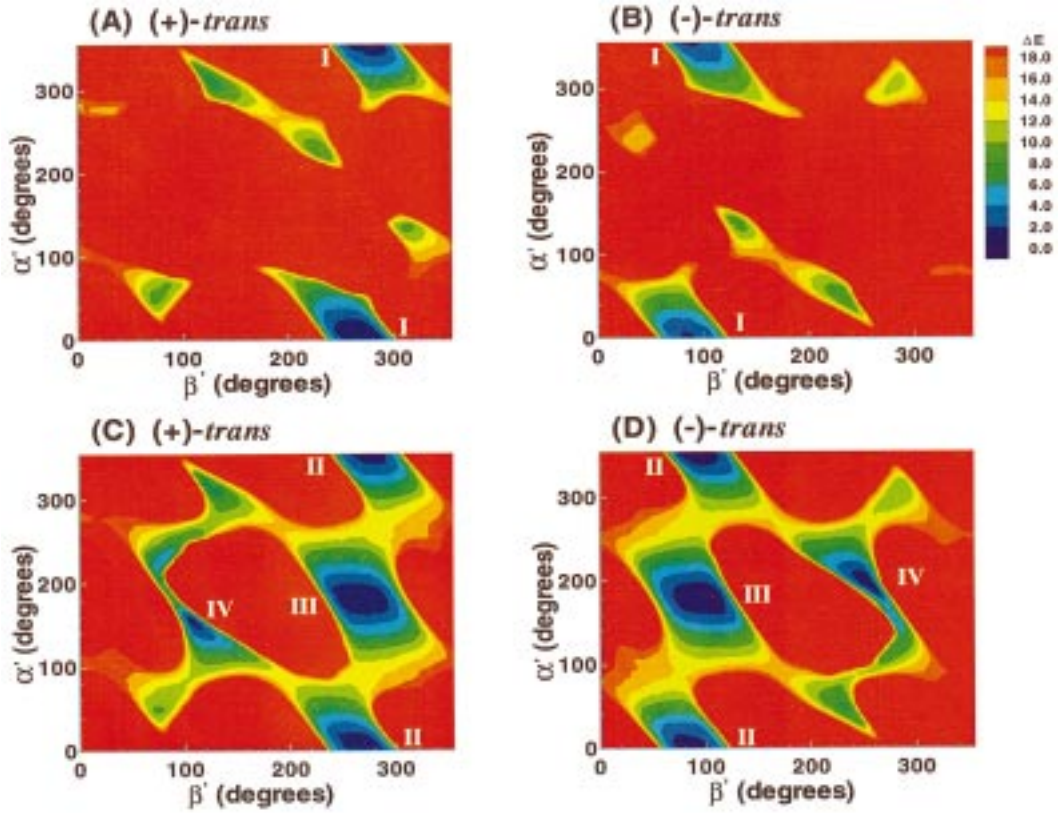

FIGURE 3: α', β' energy contour maps to 20 kcal/mol. I−IV denote the 4 low-energy domains. Torsion angles cycle over 360°, so 359° is actually contiguous with 0°: A, (+)-*trans-anti*-[BP]-N^2-dG adduct, $\chi = 50°$ (*syn*); B, (−)-*trans-anti*-[BP]-N^2-dG adduct, $\chi = 50°$ (*syn*); C, (+)-*trans-anti*-[BP]-N^2-dG adduct, $\chi = 230°$ (*anti*); D, (−)-*trans-anti*-[BP]-N^2-dG adduct, $\chi = 230°$ (*anti*).

resides in steric hindrance effects resulting from the mirror image relationship of the BP benzylic rings in the adduct pair, such that rotation of one stereoisomer from one of its domains into the analogous conformational domain of the other causes crowding between the guanine and the BP benzylic ring. Limited conformational flexibility in the torsion angle β' about the BP(C10)−N^2(dG) covalent bond closest to the bulky BP moiety at the linkage site to guanine plays a key role in governing the energetically most favored orientations in each adduct.

METHODS

Creating Starting Conformations. Coordinates of the high-resolution NMR solution structures of the (+) and (−)-*trans-anti*-[BP]-N^2-dG adducts in a DNA duplex 11-mer (*16*, *18*) were employed to create the modified nucleoside adducts by excising the [BP]-N^2-dG adduct, including the sugar with O3′ and O5′, using the program INSIGHTII from MSI, Inc., which was also used to draw the three-dimensional structures. Hydrogens were added to the O3′ and O5′ to produce modified nucleosides. Starting structures for the energy calculations were then created with a torsion driver program which rotated the torsion angles χ, α', and β' (Figure 1) to chosen values and then computed the coordinates of the resulting structures. The starting structures uniformly surveyed the potential energy surface of the molecule with conformers in which χ, α', and β' sampled their 360° conformation space at 5° intervals, in combination, giving a total of $(360/5 = 72)^3 = 373248$ conformers for each adduct. The C4′−C5′ bond and the sugar pucker were maintained in the conformation they had adopted in the B-DNA duplex from which the nucleosides had been excised. Values of the sugar pseudorotation parameter **P** (*34*) are 150° and 162°, in the normal C2′-endo domain of B-DNA, for the (+) and (−) adducts, respectively. The C3′−C4′−C5′−O5′ torsion angles are normal B-DNA values of 40° and 47°, respectively, in the (+) and (−) adducts.

Table 3: Statistical Weights and Thermodynamic Parameters of Low-Energy Domains in (+) and (−)-*trans-anti*-[BP]-N^2-dG Adducts[a]

	W%		ΔG (kcal/mol)		ΔH (kcal/mol)		$T\Delta S^{-1}$ (kcal deg^{-1} mol^{-1})	
domain	(+)	(−)	(+)	(−)	(+)	(−)	(+)	(−)
I	17.0	2.1	0.63	1.92	0	1.43	0.29	0.43
II	32.5	40.4	0.24	0.15	0.41	0.28	1.09	1.05
III	48.8	48.8	0	0.14	0.33	0.33	1.25	1.21
IV	1.7	8.7	2.0	1.07	1.09	0.16	0	0.01

[a] Statistical weights, *W*, are given in percents of the population. ΔG, ΔH, and ΔS are differences in conformational free energy, enthalpy, and entropy, respectively, relative to the lowest value for either isomer.

Energy Computation. Energies of each of the 373248 structures for each adduct were computed with the molecular mechanics program AMBER 4.0 (*35*). Since there are no negatively charged phosphates in the nucleoside, Na^+ counterions were not needed. A sigmoidal distance-dependent dielectric function (*36*) which is a suitable treatment for the dielectric constant (*37*) was employed in the Coulombic term of the force field, to model the dielectric effects of solvent water. Parameters added to the AMBER 4.0 force field for the [BP]-N^2-dG adducts are the same as those in earlier work (*15*), except that new partial charges were computed with Gaussian 92 at the STO-3G basis set level which is

compatible with the rest of the AMBER 4.0 force field. Partial charges, atom types, and topology information are given in Table S1, Supporting Information.

Computations were carried out at the Department of Energy National Energy Research Computer Center (Berkeley, CA), at the National Science Foundation National Partnership for Advanced Computational Infrastructure (San Diego, CA), and on our own SGI workstations.

RESULTS

Four Conformational Domains with Quasi-mirror Image Structures in (+)-trans and (−)-trans Adducts. Figure 2 shows three-dimensional energy topographies as a function of χ, α', and β' to 5 kcal/mol for the (+) and (−)-*trans* adducts. This figure summarizes the low-energy regions computed from the complete survey of the χ, α', and β' torsion angles at 5° intervals in combination (373248 conformers for each adduct). Table 1 gives the number of conformers in each 1 kcal/mol energy shell up to 5 kcal/mol. We see immediately that there are only four low-energy domains (potential energy wells) for each of the adducts. Domain I has a *syn* glycosidic torsion angle χ, and Domains II, III, and IV are in the *anti* region. Table 2 summarizes the approximate χ, α', and β' ranges within the 5 kcal/mol surfaces in each of these four domains.

To examine in more detail the relationship between the energy landscapes of the (+) and (−) adducts as a function of the critical torsion angles α' and β' that govern the BP orientation, we made slices through the approximate centers of the wells in the χ axis to obtain energy contour maps in the α', β' plane, to 20 kcal/mol, shown in Figure 3. These reveal clearly a striking symmetry in the (+) and (−) adduct maps that is also manifest in the three-dimensional surfaces: the map for the (+) adduct can be essentially transformed into that of the (−) by inverting the sign of the torsion angles α' and β', and vice versa. This also corresponds to a 180° rotation about a central symmetry axis which is perpendicular to the map plane, at α', $\beta' = 180°$, 180°. Thus, a given energy feature in a specific α', β' region of the (+) adduct map has a corresponding feature in the (−) adduct map in the $-\alpha'$,$-\beta'$ region. The summary of the low-energy domains of Table 3 clearly indicates this feature for β', but less clearly for α' because 0° and 180°, the lowest-energy regions for α', are the same when their signs are inverted. However, the energy landscape to 20 kcal/mol, which displays additional α' regions, shows the phenomenon strikingly. Such torsion angle symmetry is a classical hallmark of mirror image pairs of molecules. However, the symmetry is not perfect in this case, as discussed below.

The α', β' energy map of Figure 3 also shows that there is much greater conformational flexibility in α' than β' in both adducts: only for α' is most of the 360° of torsion angle space accessible, lying in energy regions below the forbidden ones beyond 20 kcal/mol.

Another feature that can be discerned from the α', β' maps of Figure 3 is the pathways connecting *anti* Domains II, III, and IV to one another, at energies of about 12−16 kcal/mol. The three-dimensional χ, α', and β' energy topographies of Figure 2 suggested a path also might exist between *syn* Domain I and *anti* Domain II, along the trajectory $\chi = 335°$ (= −25°) through $\chi = 0°-15°$. To elucidate this further,

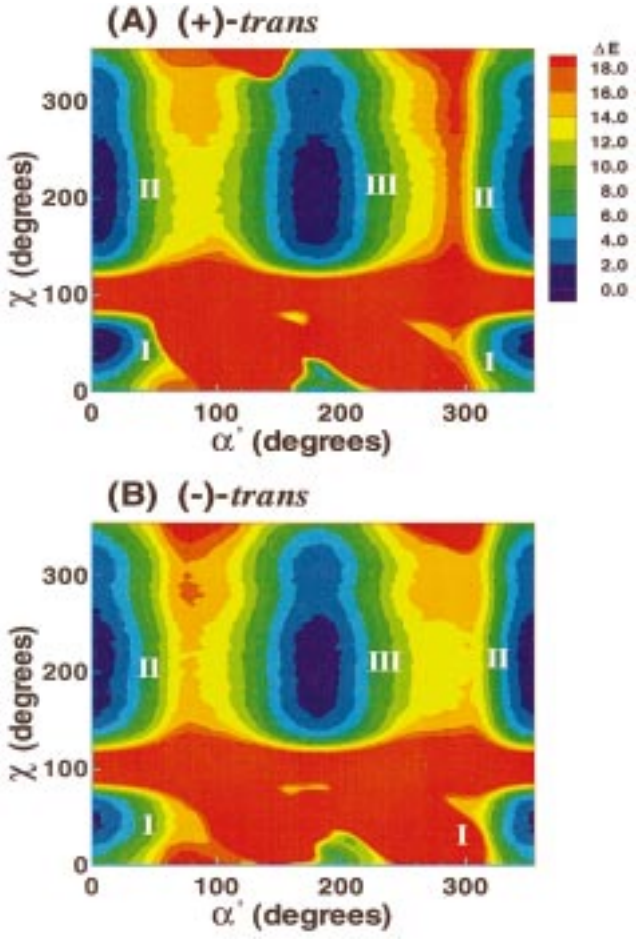

FIGURE 4: χ, α' energy contour maps to 20 kcal/mol with $\beta' = -90°$ for (+) adduct and 85° for (−) adduct. I−III denote 3 low-energy domains. Torsion angles cycle over 360°, so 359° is actually contiguous with 0°: A, (+)-*trans-anti*-[BP]-N^2-dG; adduct B, (−)-*trans-anti*-[BP]-N^2-dG adduct.

we made a two-dimensional energy contour slice through the approximate centers of Domains I and II, at $\beta' = 270°$ (−90°) for the (+)-*trans* adduct and 85° for the (−)-*trans* adduct. This map, shown in Figure 4, reveals the path at about 7 kcal/mol, involving the rotation of χ from about 335° through 0° to about 15°. This figure shows Domains I, II, and III, but Domain IV does not exist in the β' slices employed in these maps. These paths represent upper energy limits since our computations could only survey the key χ, α', and β' flexibility sources. Still, they suggest that interconversion between domains would be slow, as a consequence of the bulk of the BP.

Steric Hindrance Origins of Opposite Orientations. To elucidate whether the symmetry between the (+) and (−) adduct energy contour maps as a function of α' and β' (Figures 2 and 3) resides in steric repulsion, we prepared α', β' contour maps for each adduct with just the van der Waals component of the total energy (Figure 5). These maps reveal the same overall symmetry effects as Figure 3. The overall shapes of the regions below 20 kcal/mol are governed by the high-energy bounds above this energy; these high energy bounds are determined by repulsive steric components of the Lennard−Jones potential employed to compute van der Waals energies (*38*). Therefore, steric repulsions are responsible for the starkly different energy landscapes in the (+) and (−)-*trans* adducts and for the symmetries between

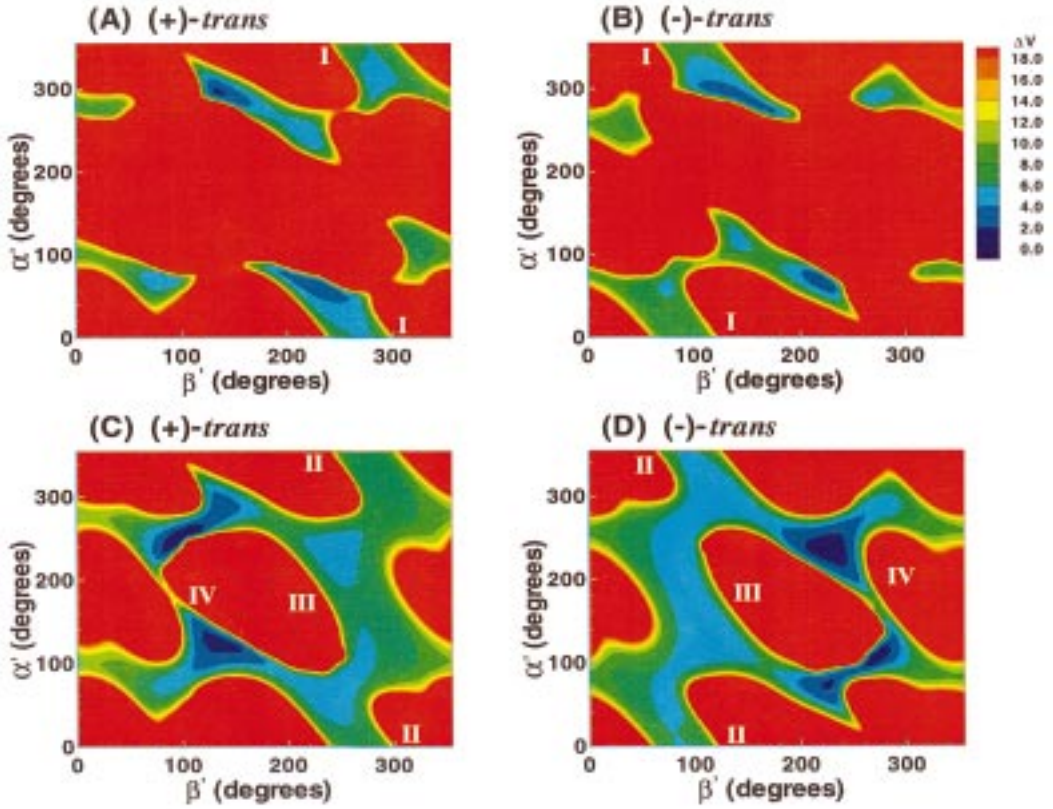

FIGURE 5: α', β' van der Waals energy component maps to 20 kcal/mol. I−IV denote the 4 low-energy domains. Torsion angles cycle over 360°, so 359° is actually, contiguous with 0°: A, (+)-*trans-anti*-[BP]-N^2-dG adduct, $\chi = 50°$ (*syn*); B, (−)-*trans-anti*-[BP]-N^2-dG adduct, $\chi = 50°$ (*syn*); C, (+)-*trans-anti*-[BP]-N^2-dG adduct, $\chi = 230°$ (*anti*); D, (−)-*trans-anti*-[BP]-N^2-dG adduct, $\chi = 230°$ (*anti*).

them, although small differences in detail stem from the nonmirror image nature of the sugars and attached C4′−C5′ groups (see below).

Figure 6 shows color views of representative structures of each of the four low-energy domains for the (+) and (−) adduct. Figures 7 and 8 show these structures in stereo. Figure 6 shows that for each domain the (+)-*trans* adduct structure is a mirror image of the (−)-*trans* structure, with the mirror image symmetry broken by the sugars and attached C4′−C5′ group. The nonmirror image nature of the sugars can be discerned by noting that the sugar O4′ atoms point in the same rather than the opposite direction for the (+) and (−)-*trans* adducts in each domain. However, breaking of the mirror image symmetry by the sugars and C4′−C5′ groups has only a small effect on the energy contour maps in the *anti* domain because the sugars are farther from the guanine and BP moiety than in the *syn* conformation. In *syn* Domain I, interactions between the guanine and its attached BP with the sugar are greater because the base lies over the sugar and C4′−C5′ group.

The four structural types are approximately related by torsional rotations as follows:

$$\text{Domain I} \xrightarrow{\chi + \sim 180^\circ} \text{Domain II}$$

$$\text{Domain II} \xrightarrow{\alpha' + \sim 180^\circ} \text{Domain III}$$

$$\text{Domain III} \xrightarrow{\beta' + \sim 180^\circ} \text{Domain IV}$$

Syn Domain I differs from *anti* Domain II in orientation of the sugar relative to guanine. An ∼180° rotation of α', which converts Domain II to Domain III, turns the BP long axis in the opposite direction. An ∼180° rotation in β' then produces Domain IV, in which the BPs are directed as in Domain II, but the bay region of the BP is at the top in Domain IV and at the bottom in Domain II in the view of Figure 6.

To investigate why the structures in a given domain for the (+)-*trans* adduct are disfavored for the (−)-*trans* adduct, and vice versa, we rotated each structure in Figure 6 into that of its stereoisomer. This entailed a 180° rotation around β' in each case. Results are shown in Figures 9 and 10. Placing β' in the wrong conformation for the given isomer causes crowding between guanine and BP, involving especially the benzylic ring and adjacent aromatic rings in the bay region, except in Domain IV. In rotated Domains I and II the guanine N1 edge is in the crowded region, and in Domain III the guanine N3 edge is crowded. Note, however, that the Domain IV structure of the (+) adduct is similar to the Domain III structure of the (−) isomer, and likewise, the Domain IV structure of the (−) isomer is like the Domain III structure of the (+) isomer, although with some adjustment (Table 2 and Figure 3). Table 2 shows the α', β' relationships among the domains. Figures 2, 3, and 5 also reveal that the low energy domains of the (+)-*trans* adduct are high-energy for the (−)-*trans* and vice versa, and Figure 5 pinpoints steric hindrance as the source of the opposite orientation phenomenon.

Statistical Weights and Thermodynamic Parameters. We computed the fractional statistical weight together with relative conformational free energies, enthalpies and entropies for each domain of the (+) and (−) adduct, as described in the Appendix, using standard definitions (*38*). Table S2 (Supporting Information) gives the G, H and TS values used

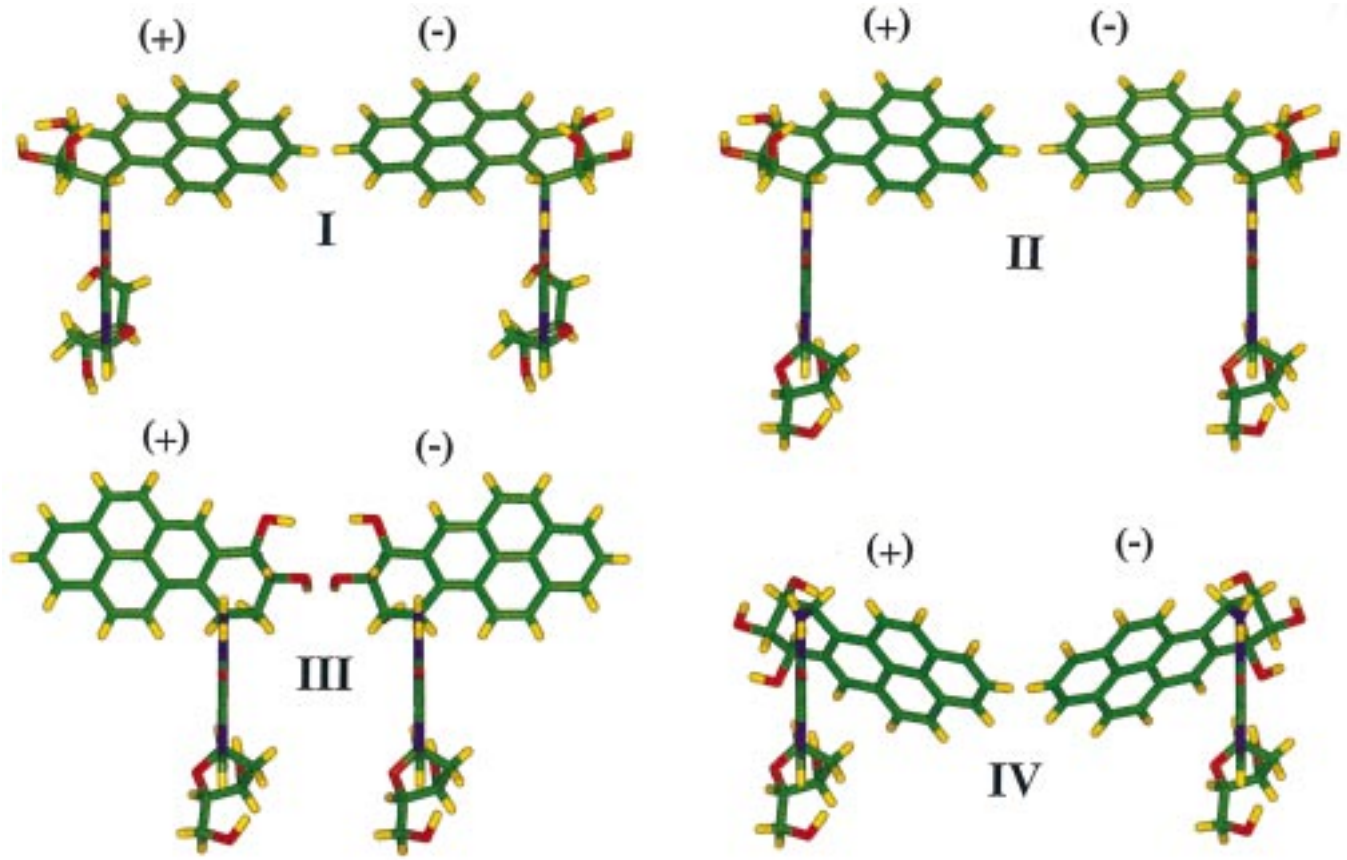

FIGURE 6: Color views of representative structures for (+) and (−)-*trans-anti*-[BP]-N^2-dG adducts. I−IV denote 4 low-energy domains. In each pair the left structure is the (+) adduct and the right is the (−) one. χ, α', and β' values and energies, ΔE, relative to the global minimum are the following. Domain I: (+) adduct 50°, 0°, 270°; (−) adduct 50°, 0°, 90°; ΔE (+) 0.33, (−) 1.91 kcal/mol. Domain II: (+) adduct 230°, 0°, 270°; (−) adduct 230°, 0°, 90°; ΔE (+) 0.89, (−) 0.90 kcal/mol. Domain III: (+) adduct 230°, 180°, 270°; (−) adduct 230°, 180°, 90°; ΔE (+) 0.54, (−) 0.85 kcal/mol. Domain IV: (+) adduct 230°, 155°, 110°; (−) adduct 230°, −155°, −110°; ΔE: (+) 1.34, (−) 1.05 kcal/mol. The view is edge-on along the guanine with O6 directed toward the viewer.

to compute Table 3. Computation of these thermodynamic parameters for each domain treats these as individual chemical species, which is justifiable on the basis of the high barrier between the domains (Figures 3 and 4). Results are given in Table 3. We note that about 80−90% of the conformers occupy either Domain II or III, with Domain III containing the highest population. Differences in population and other quantities between the (+) and the (−) adduct stem from the symmetry breaking effect of the sugar and C4′−C5′, which has the greatest effect in *syn* Domain I where the base lies over the sugar and C4′−C5′ group.

DISCUSSION

Quasi-Mirror Image Symmetries and Opposite Orientations. Our computations have revealed four pairs of low-energy conformational domains for the (+) and (−)-*trans-anti*-[BP]N^2-dG adducts, Domains I, II, III and IV. In each domain the pyrenyl moieties adopt a mirror image symmetry as viewed along the O6-containing guanine edge in the (+) and (−) adduct pair, resulting in opposite orientations of the BP (Figure 6). The mirror image symmetry between the (+) and (−) BP moieties is broken by the sugars with their attached C4′−C5′ group. The energy landscape of the two adducts reveal this mirror image symmetry; they are transformable into one another by sign inversion of α' and β', corresponding to rotation about a central symmetry axis perpendicular to the map plane located at $\alpha',\beta' = 180°, 180°$ in Figure 3. The inversion in the signs of α' and β' for the corresponding low-energy domains in the (+) and (−) adducts, a hallmark of mirror image symmetry, is rooted in the exact mirror image nature of the BP benzylic ring in the two adducts. The mirror image breaking effect of the sugars and their attached C4′−C5′ groups has the greatest impact on the energy landscape in the *syn* Domain I, in which the base and its attached BP are closest to the sugar and its attached C4′−C5′ group. The Domain IV structure is also a more crowded one and more affected by the sugar. Differences between the two isomers in conformational enthalpies and free energies (Table 3) are greatest in these two domains for this reason. The Domains II and III structures are more extended than those of Domains I and IV, and their energy landscapes are less affected by the sugars. They are the two most favored domains in both adducts (Table 3); their extended nature produces more flexible structures which corresponds to more favorable conformational entropies. This is manifested in the larger number of conformers in the low-energy 1 kcal/mol shells (Table 1) as compared to Domains I and IV. Domain III appears to be favored over Domain II because the N1H1 edge of guanine is directed to the opposite side of the benzylic ring O9H in Domain III, while it is directed to the same side in Domain II; this likely causes the diminished conformational flexibility, with fewer low-energy conformers (Table 1), in Domain II. Thus, differences in domain occupancies between (+) and (−) adducts (Table

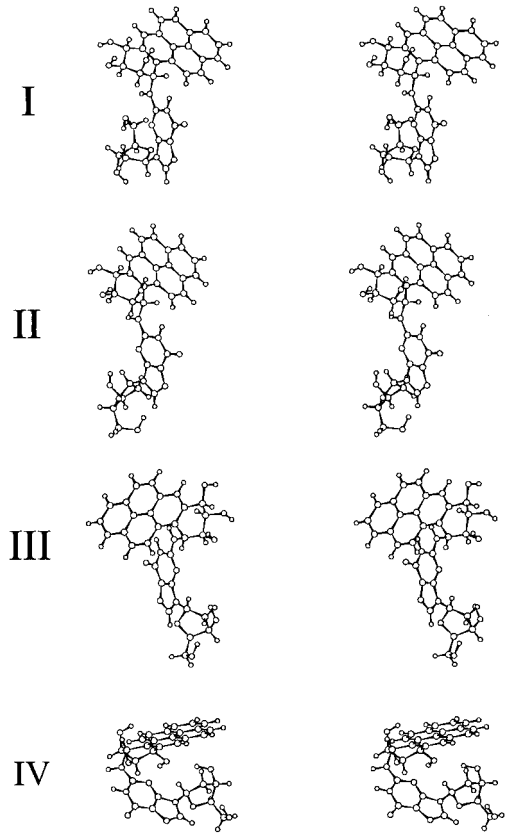

FIGURE 7: Stereoviews for (+)-*trans-anti*-[BP]-N^2-dG adduct. Representative structures of Figure 6. I−IV denote 4 low-energy domains.

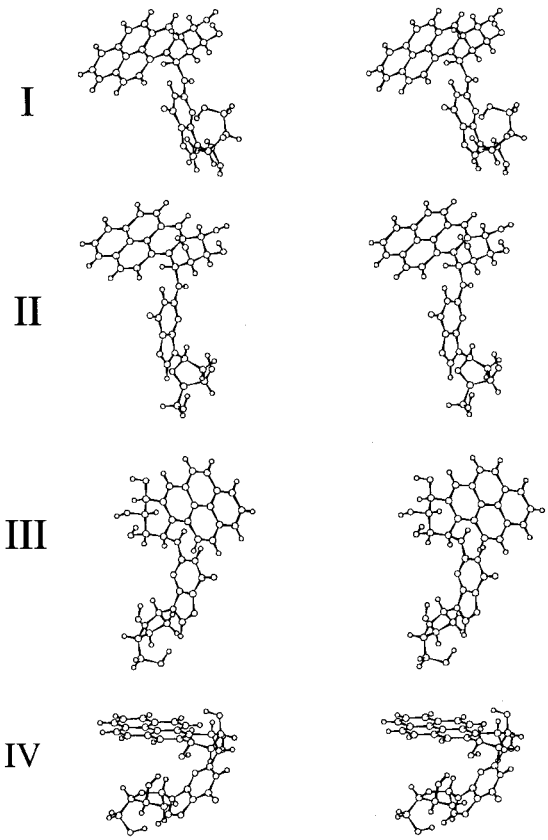

FIGURE 8: Stereoviews for (−)-*trans-anti*-[BP]-N^2-dG adduct. Representative structures of Figure 6. I−IV denote 4 low-energy domains.

3) are enthalpic in origin, resulting from the differing energetic interactions between sugar/C4′−C5′ and the guanine with its attached benzo[a]pyrenyl moiety; however, differences in domain occupancies for each isomer are governed by both entropic contributions from the differing degrees of conformational flexibility allowed in the different domain structures, and enthalpic contributions (Tables 1, 3).

In the low-energy domains, α′ is de facto the same for the (+) and (−) adducts (Table 2); consequently, rotation of just β′ to its sign inverted value (β′ to −β′) brings the structure of one isomer into that of the other. Steric crowding between the base and the BP, especially the benzylic ring, ensues in each domain. Crowding between adduct components within the modified nucleoside has been termed "primary" steric hindrance (*21*). Torsion angle β′ thus plays a key role in the conformations of the two isomers, first because α′ is invariant under sign inversion in the low-energy domains, and second, because β′ has much more limited flexibility than α′ (Figure 3) since it is closer to the bulky BP. Thus, one would anticipate that primary steric hindrance effects would play an important part in keeping β′ out of high-energy regions (Figure 3) and near the region that is favored for each isomer. The extent to which this has been observed so far is discussed below.

Preferred Domains and Relevance to Opposite Orientations in DNA Duplexes. Our results are specifically relevant to embedding the BP-modified nucleosides into B-DNA since we employed the C2′-endo sugar pucker and C4′−C5′ bond orientations found predominantly in B-DNA (*39*). Nucleosides can manifest additional conformational flexibilities (*40, 41*). Nonetheless, it is quite striking that the structures of DNA duplexes containing the (+) and (−)-*trans-anti*-[BP]-N^2-dG adducts investigated in the present work on the nucleoside level are in or very close to the χ, α′, and β′ torsion angle regions found for our most favored, oppositely oriented Domain III structures for each [BP]-N^2-dG mononucleoside adduct (Table 2). Table 4 gives these torsion angle values for both the normal full duplex structures (*16, 18*) and the 11/10-mer "deletion" duplexes (*19, 20*) found in our earlier work; it reveals that the α′, β′ torsion angles in the two types of duplexes are very similar in each adduct. This is true despite the fact that the two types of structures are altogether different: the full duplexes contain BP moieties which are in the minor groove, while the deletion duplexes contain base displaced-intercalated structures. In both cases, however, the BP moieties are oppositely oriented, relative to the 5′ or 3′ direction of the modified strand in the full duplexes, and relative to the major or minor groove side of the helix cylinder in the deletion duplexes, as detailed in the introduction. The differing positions of the BP in the two kinds of duplexes stem from a number of differences in DNA backbone torsion angles in residues immediately adjacent to the modification (*42*). The Domain III α′ region centered at 180° is preserved in the "deletion" duplexes even though the base displaced-intercalation structures have no Watson−Crick base pairing, which requires α′ near 180° (*21*). Thus, this domain is intrinsically favored apart from any further stabilization that would result from base pairing. Domain III was also observed in the solution structure of the (+) adduct at a single strand/double strand junction in which a partner cytidine residue was present opposite the [BP]dG (*43*). In this case a normal B-form was preserved at

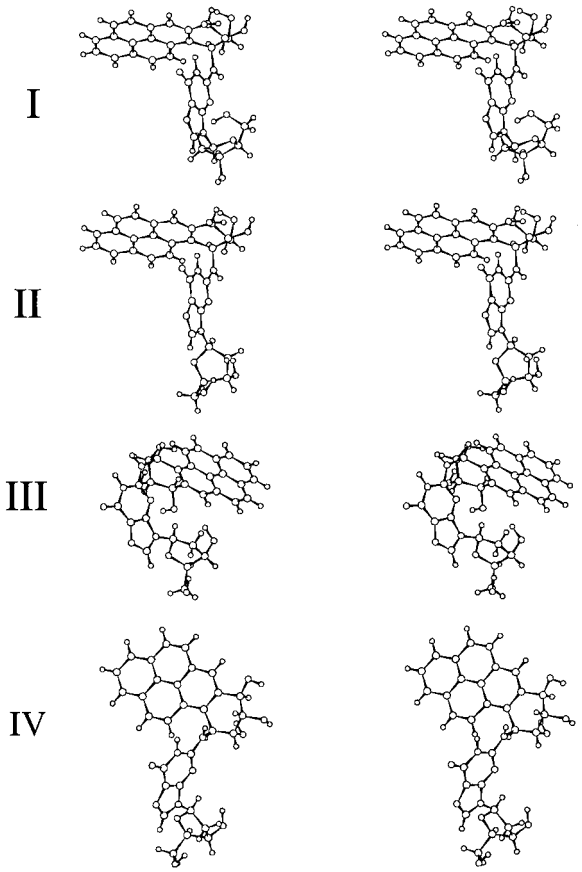

FIGURE 9: Stereoviews of (+) adduct structures rotated to wells of (−) adduct as detailed in Figure 6. I−IV denote 4 low-energy domains.

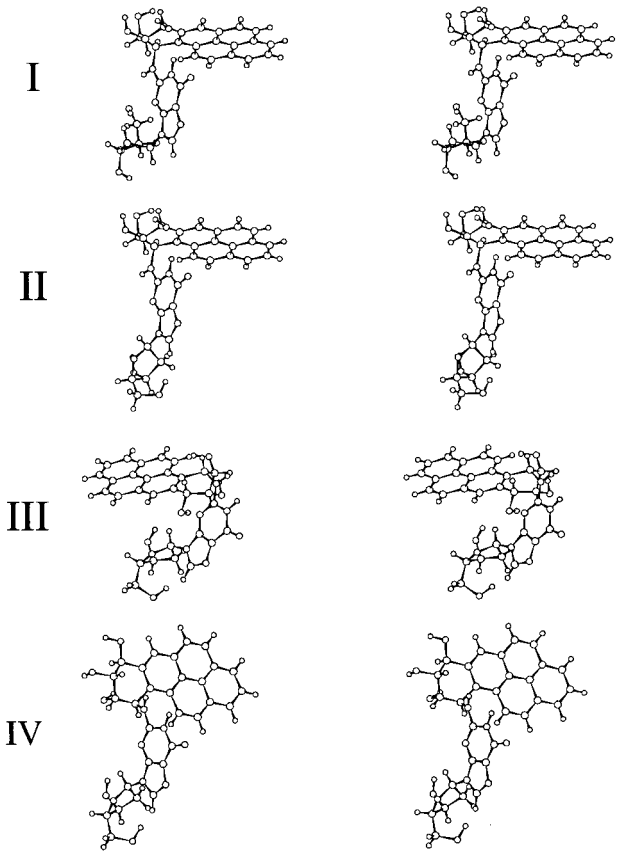

FIGURE 10: Stereoviews of (−) adduct structures rotated to wells of (+) adduct as detailed in Figure 6. I−IV denote 4 low-energy domains.

the modified residue, and χ, α', and β' were centered at 269°, 196°, 278°, respectively, in the NMR ensemble. However, in the solution structure of a single strand/double strand junction with (+) adduct at the junction, but no partner cytosine present, the B-DNA conformation was not preserved at the modified residue, with a wide array of sugar puckers differing very substantially from the B-DNA C2′-endo region in the ensemble of NMR structures (*44*). The glycosidic torsion angle χ is *syn* in these structures (*21, 44*), but their energies cannot be deduced from our energy landscapes which were computed only for the C2′-endo sugar pucker. In this very flexible situation it was possible for interactions between the hydrophobic pyrenyl rings and the mobile single-stranded region to satisfy the BP hydrophobicity, and this is not possible in more constrained duplex structures.

Finally, we consider the possibility of overcoming the opposite orientation proclivity in (+) and (−)-*trans-anti* adduct pairs and the significance of Domain IV. We note that the Domain III χ, α', and β' values and BP orientations for the (+) adduct are rather similar to the Domain IV values for the (−), and vice versa (Table 2, Figures 3 and 6), although with some adjustment. Domain IV has a low probability, but its existence leaves open the possibility that it could become more favored in particular environmental situations, including larger structures, differing neighbor sequences, and the presence of a polymerase enzyme. An exquisite dependence of conformational balance on neighboring sequence has recently been shown for another bulky adduct, 2-aminofluorene to guanine C8 (*45*−*47*). This possibility for occupancy of Domain IV, in which the orientation of the BP moiety is rotated oppositely compared to the most favored Domain III, may contribute to an understanding of the observation that a given adduct can produce different kinds of mutations in differing sequence contexts (*48*−*55*).

Table 4: χ, α', β' Orientation in NMR Solution Structures of (+) and (−)-*trans-anti*-[BP]-N^2-dG Adducts

duplex type	χ, α', β' (deg) (+)	(−)
normal partner	257, 137, 258[a]	260, 152, 78[b]
partner residue missing	301, 138, 263[c]	179, 178, 94[d]

[a] Cosman et al. (*16*); 258° = −102°. [b] de los Santos et al. (*18*). [c] Cosman et al. (*19*); 263° = −97°. [d] Feng et al. (*20*).

Of particular interest are recent site-directed mutagenesis experiments in various cell systems, including mammalian cells (*51, 54*), using defined *anti*-[BP]-N^2-dG adducts, which show that a particular stereochemically defined adduct can give rise to more than one kind of mutation and is base sequence-dependent (*51*−*55*). There are indications that the conformations of *anti*-[BP]-N^2-dG lesions depend on sequence context (*16, 17, 56*; reviewed in ref *21*), especially at template/primer replication fork model systems (*43, 44*). Loechler and co-workers (*48*−*50, 57*−*59*) have proposed that the different kinds of mutations engendered by the same stereochemically defined *anti*-[BP]-N^2-dG adduct may be due to the coexistence of multiple conformations. Whatever these conformations may be, our results strongly suggest that primary steric hindrance effects limit the range of allowable

conformations, especially the relative orientations of the dG and BP residue ring systems.

CONCLUSION

The mirror image symmetry in the (+) and (−) pair of mononucleoside adducts at the level of guanine base linked to BP produces four mirror image pairs of structural types with the symmetry broken by the sugar and C4′−C5′ group at the nucleoside level. About 80−90% of the population is occupied by two pairs of structures, Domain II and Domain III. Domain III, the most favored, represents the domain actually observed so far in DNA duplexes for each of the adducts. Thus, the mirror image symmetry manifested only at the guanine-BP adduct level and rooted in the mirror image nature of the benzylic rings in the (+) and (−) adducts is sufficiently forceful in primary steric interactions to be retained in DNA duplexes, resulting in the observed opposite orientations of the (+) and (−)-*trans-anti* adduct pairs in duplexes (*16*−*20*). The opposite orientation phenomenon could manifest itself when the adducts are processed by cellular enzymes because it is a direct consequence of primary steric hindrance effects. Thus, repair, replication, or transcription enzymes could process the (+) and (−)-*trans-anti*-[BP]-N^2-dG lesions differently. In vitro exonuclease digestion studies by Mao et al. (*60*) have already revealed such differential processing. Moreover, our finding of a low but real probability for overcoming the opposite orientation proclivity in our Domain IV structures might contribute toward explaining mutagenic hotspot sequences in vivo (*49*), if such hotspots are characterized by conformations that differ from those at coldspots, as has been hypothesized (*48, 49*). However, other conformational rearrangements such as exchanges between minor groove type orientations and base displaced-intercalated orientations could well play an important role in defining hotspots (*21, 47, 58, 59, 61*). Whatever the conformations may be, primary steric hindrance effects are likely to limit the range of allowable orientations of the BP residue relative to the DNA. Moreover the methods developed here offer the opportunity to elucidate other systems by a similar approach.

ACKNOWLEDGMENT

We thank Prof. Robert Topper, the Cooper Union for the Advancement of Science and Art, and Prof. Wilma Olson, Chemistry Department, Rutgers University, for very helpful discussions and advice.

SUPPORTING INFORMATION AVAILABLE

Two tables, one listing partial charges, topology, and atom type assignments for the (+) and (−)-*trans-anti*-[BP]-N^2-dG adducts and the other giving G, H, and TS values used to compute Table 3, and two figures showing the full set of α′, β′ energy contour maps at 5° intervals of χ for the (+) and (−)-*trans-anti*-[BP]-N^2-dG adducts, respectively. This material is available free of charge via the Internet at http://pubs.acs.org.

APPENDIX

Computation of Statistical Weights, Thermodynamic Quantities, and Energy Maps. The fractional statistical weight, P_i of each conformer was computed from the relationship

$$P_i = \frac{e^{-\Delta E_i/RT}}{\sum_{i=1}^{N} e^{-\Delta E_i/RT}}$$

where ΔE_i is the relative energy of a given conformer in kcal/mol with respect to the lowest-energy structure; R is the universal gas constant, 1.987×10^{-3} kcal/mol; $T = 300°$ K; and N is 373248, the total number of conformers for each adduct.

The energies were used to construct both three-dimensional energy surfaces as a function of the χ, α′, and β′ torsion angles and two-dimensional energy contour slices through them; slices were made at 5° intervals of χ as a function of α′, β′, and also at selected β′ values as a function of χ, α′. The program TECPLOT was used for this purpose. These plots revealed four low-energy wells or domains (Figure 2, and Supporting Information Figures S1 and S2). This permitted grouping the full data set into four regions, each of which encompassed one of the four low-energy domains:

Region 1: χ = 0°−100°; α′ = 0°−100° and 285°−355°; β′ for (+) adduct = 185°−355°; β′ for (−) adduct = 0°−175°

Region 2: χ = 105°−355°; α′ = 0°−100° and 285°−355°; β′ for (+) adduct = 185°−355°; β′ for (−) adduct = 0°−175°

Region 3: χ = 0°−355°; α′ = 105°−280°; β′ for (+) adduct = 185°−355°; β′ for (−) adduct = 0°−175°

Region 4: χ = 0°−355°; α′ = 0°−355°; β′ for (+) adduct = 0°−180°; β′ for (−) adduct = 180°−355°

With this grouping, we computed the combined fractional statistical weight, W_j, for each region (containing one low-energy well) by summing the individual statistical weights, P_i, of each point in the region:

$$W_j = \sum_{i=1}^{n_j} P_i$$

where n_j is the number of conformers in each one of the four regions (j = 1, 2, 3, 4). In practice, only conformers with energies ΔE_i below 3 kcal/mol contribute significantly to the fractional statistical weight of a given region, but all conformers in the region were included in the calculation.

The conformational free energy of each well, G_j, was then computed from the relationship

$$G_j = -RT \ln \sum_{i=1}^{n_j} e^{-\Delta E_i/RT}$$

To obtain the conformational entropy of each well, S_j, we first compute p_i, the fractional statistical weight of each conformer within its own well or region:

$$p_i = \frac{e^{-\Delta E_i/RT}}{\sum_{i=1}^{n_j} e^{-\Delta E_i/RT}}$$

$$S_j = -R \sum_{i=1}^{n_j} p_i \ln p_i$$

Conformational enthalpies for each well, H_j, are then obtained from

$$G_j = H_j - TS_j$$

REFERENCES

1. Harvey, R. G. (1991) *Polycyclic Aromatic Hydrocarbons: Chemistry and Carcinogenicity*. Cambridge University Press.
2. Grimmer, G. (1993) Relevance of polycyclic aromatic hydrocarbons as environmental carcinogens. *Proceedings of the 13th International Symposium on Polynuclear Aromatic Hydrocarbons* (Garrigues, P., and Lamotte, M., Eds.) pp 31−41, Gordon and Breach Science Publishers, Langhorne, PA.
3. Perrin, J. L., Poirot, N., Liska, P., Hanras, C., Theinpont, A., and Felix, G. (1993) Trace enrichment and HPLC analysis of PAHs in edible oils and fat products, using liquid chromatography on electron acceptor stationery phases in connection with reverse phase and fluorescence detection. *Proceedings of the 13th International Symposidum on Polynuclear Aromatic Hydrocarbons*, (Garrigues, P., and Lamotte, M., Eds.) pp 337−346, Gordon and Breach Science Publishers, Langhorne, PA.
4. Conney, A. H. (1982) Induction of microsomal enzymes by foreign chemicals and carcinogenesis by polycyclic aromatic hydrocarbons. *Cancer Res. 42*, 4875−4917.
5. Vousden, K. H., Bos, J. L., Marshall, C. J., and Philips, D. H. (1986) Mutations activating human C−Ha-*rasI* protooncogene (HRASI) induced by chemical carcinogens and depurination. *Proc. Natl. Acad. Sci.U.S.A. 83*, 1222−1226.
6. Denissenko, M. F., Pao, A., Tang, M.-S., and Pfeifer G. P. (1996) Preferential formation of benzo[*a*]pyrene adducts at lung cancer mutational hotspots in *P53*. *Science 274*, 430−432.
7. Buening, M. K., Wislocki, P. G., Levin, W., Yagi, H., Thakker, D. R., Akagi, H., Koreeda, M., Jerina, D. M., and Conney, A. H. (1978) Tumorigenicity of the optical enantiomers of the diastereomeric benzo[a]pyrene 7,8-diol-9,10-epoxides in newborn mice: exceptional activity of (+)-7β,8α-dihydroxy-9α,10α-epoxy-7,8,9,10-tetrahydrobenzo[a]pyrene. *Proc. Natl. Acad. Sci. U.S.A. 75*, 5358−5361.
8. Slaga, T. J., Bracken, W. J., Gleason, G., Levin, W., Yagi, H., Jerina, D. M. and Conney, A. H. (1979) Marked differences in the skin tumor-initiating activities of the optical enantiomers of the diastereomeric benzo[a]pyrene 7,8-diol-9,10-epoxides. *Cancer Res. 39*, 67−71.
9. Brookes, P., and Osborne, M. R. (1982) Mutation in mammalian cells by stereoisomers of *anti*-benzo[a]pyrene diol epoxide in relation to the extent and nature of the DNA reaction products. *Carcinogenesis 3*, 1223−1226.
10. Meehan T., and Straub, K. (1979) Double stranded DNA stereoselectively binds benzo[a]pyrene diol epoxides. *Nature 277*, 410−412.
11. Cheng, S. C., Hilton, B. D., Roman, J. M., and Dipple, A. (1989) DNA adducts from carcinogenic and noncarcinogenic enantiomers of benzo[a]pyrene dihydrodiol epoxide. *Chem. Res. Toxicol. 2*, 334−340.
12. Weinstein, I. B., Jeffrey, A. M., Jennette, K. W., Blobstein, S. H., Harvey, R. G., Harris, C., Autrup, H., Kasai, H., and Nakanishi, K. (1976) Benzo[a]pyrene diol epoxides as intermediates in nucleic acid binding *in vitro* and *in vivo*. *Science 193*, 592−594.
13. Jeffrey, A. M., Jennette, K. W., Blobstein, S. H., Weinstein, I. B., Beland, F. A., Harvey, R. G., Kasai, H., Miura, I., and Nakanishi, K. (1976) Benzo[a]pyrene-nucleic acid derivative found *in vivo*: structure of benzo[a]pyrenetetrahydrodiol epoxide-guanosine adduct. *J. Am. Chem. Soc. 98*, 5714−5715.
14. Osborne, M. R., Beland, F. A., Harvey, R. G., and Brookes, P. (1976) The reaction of (+)-7α,8β-dihydroxy-9β,10β-epoxy-7,8,9,10-tetrahydrobenzo[a]pyrene with DNA. *Int. J. Cancer 18*, 362−368.
15. Singh, S. B., Hingerty, B. E., Singh, U. C., Greenberg, J. P., Geacintov, N. E., and Broyde, S. (1991) Structures of the (+) and (−)-*trans-anti*-BPDE adducts to guanine-N^2 in a duplex dodecamer. *Cancer Res. 51*, 3482−3492.
16. Cosman, M., de los Santos, C., Fiala, R., Hingerty, B. E., Ibanez, V., Margulis, L. A., Live, D., Geacintov, N. E., Broyde, S., and Patel, D. J. (1992) Solution conformation of the major adduct between the carcinogen (+)-*anti*-benzo[a]pyrene diol epoxide and DNA. *Proc. Natl. Acad. Sci. U.S.A. 89*, 1914−1918.
17. Fountain, M. A., and Krugh, T. R. (1995) Structural characterization of a (+)-*trans-anti*-benzo[a]pyrene-DNA adduct using NMR, restrained energy minimization and molecular dynamics. *Biochemistry 34*, 3152−3161.
18. de los Santos, C., Cosman, M., Hingerty, B. E., Ibanez, V., Margulis, L. A., Geacintov, N. E., Broyde, S., and Patel, D. J. (1992) Influence of benzo[a]pyrene diol epoxide chirality on solution conformations of DNA covalent adducts: the (−)-*trans-anti*-[BP]G·C adduct structure and comparison with the (+)-*trans-anti*-enantiomer. *Biochemistry 31*, 5245−5252.
19. Cosman, M., Fiala, R., Hingerty, B. E., Amin, S., Geacintov, N. E., Broyde, S., and Patel, D. J. (1994) Solution conformation of the (+)-*trans-anti*-[BP]dG adduct opposite a deletion site in a DNA duplex: intercalation of the covalently attached benzo[a]pyrene into the helix with base displacement of the modified deoxyguanosine into the major groove. *Biochemistry 33*, 11507−11517.
20. Feng, B., Gorin, A., Kobanovskiy, A., Hingerty, B. E., Geacintov, N. E., Broyde, S., and Patel, D. J. (1997) Solution conformation of the (−)-*trans-anti*-[BP]dG adduct opposite a deletion site in a DNA duplex: intercalation of the covalently attached benzo[a]pyrene into the helix with base displacement of the modified deoxyguanosine into the minor groove. *Biochemistry 36*, 13780−13790.
21. Geacintov, N. E., Cosman, M., Hingerty, B. E., Amin, S., Broyde, S., and Patel, D. J. (1997) NMR solution structures of stereoisomeric polycyclic aromatic carcinogen-DNA adducts: principles, patterns and diversity. *Chem. Res. Toxicol. 10*, 111−146.
22. Jerina, D. M., Sayer, J. M., Yeh, H. J. C., Liu, X., Yagi, H., Schurter, E., and Gorenstein, D. (1997) NMR conformational analysis of DNA duplexes containing diol epoxide adducts of polycyclic aromatic hydrocarbons. *Polycyclic Aromat. Hydrocarbons 10*, 145−152.
23. Zegar, I. S., Setayesh, F. R., DeCorte, B. L., Harris, C. M., Harris, T. M., and Stone, M. P. (1996) Styrene oxide adducts in an oligodeoxynucleotide containing the human *N-ras* codon 12 sequence: structural refinement of the minor groove *R*(12,2)- and *S*(12,2)-α-(*N*^{2}-guanyl) stereoisomers from ^{1}H NMR. *Biochemistry 35*, 4334−4348.
24. Feng, B., Zhou, L., Passarelli, C. M., Harris, T. M., and Stone, M. P. (1995) Major groove (*R*)-α-(N^6-adenyl)styrene oxide adducts in oligodeoxynucleotide containing the human N-ras codon 61 sequence: conformation of the *R*(61,2) and *R*(61,3) sequence isomers from 1H NMR. *Biochemistry 34*, 14021−14036.
25. Feng B., Voehler M., Zhou L., Passarelli C. M., Harris T. M.; Stone M. P. (1996) Major groove *S*-α-(N^6-adenyl)-styrene oxide adducts in an oligodeoxynucleotide containing the human N-ras codon 61 sequence: conformations of the *S*(61,2) and *S*(61,3) sequence isomers from 1H NMR. *Biochemistry 35*, 7316−7329.
26. Cosman, M., de los Santos, C., Fiala, R., Hingerty, B. E., Ibanez, V., Luna, E., Harvey, R. G., Geacintov, N. E., Broyde, S., and Patel, D. (1993) Solution conformation of the (+)-*cis-anti*-[BP]dG adduct in a DNA duplex: intercalation of the covalently attached benzo[a]pyrenyl ring into the helix and

displacement of the modified deoxyguanosine. *Biochemistry 32*, 4145−4155.
27. Cosman, M., Fiala, R., Hingerty, B. E., Amin, S., Geacintov, N. E., Broyde, S., and Patel, D. J. (1994) Solution conformation of the (+)-*cis-anti*-[BP]dG adduct opposite a deletion site in a DNA duplex: intercalation of the covalently attached benzo[a]pyrene into the helix with base displacement of the modified deoxyguanosine into the minor groove. *Biochemistry 33*, 11518−11527.
28. Cosman, M., Hingerty, B. E., Luneva, N., Amin, S., Geacintov, N. E., Broyde, S., and Patel, D. J. (1996) Solution conformation of the (−)-*cis-anti*-benzo[a]pyrenyl-dG adduct opposite dC in a duplex: intercalation of the covalently attached BP ring into the helix with base displacement of the modified deoxyguanosine into the major groove. *Biochemistry 35*, 9850−9863.
29. Cosman, M., Fiala, R., Hingerty, B., Laryea, A., Lee, H., Harvey, R. G., Amin, S., Geacintov, N. E., Broyde, S., and Patel, D. (1993) Solution conformation of the (+)-*trans-anti*-[Bph]dA adduct opposite dT in a DNA duplex: intercalation of the covalently attached benzo[c]phenanthrene to the 5′-side of the adduct site without disruption of the modified base pair. *Biochemistry 32*, 12488−12497.
30. Cosman, M., Laryea, A., Fiala, R., Hingerty, B. E., Amin, S., Geacintov, N. E., Broyde, S., and Patel, D. J. (1995) Solution conformation of the (−)-*trans-anti*-[BPh]dA opposite dT adduct in a DNA duplex: intercalation of the covalently attached benzo[c]phenanthrenyl residue to the 3′-side of the adduct site and comparison with the (+)-*trans-anti*-[BPh]dA opposite dT. *Biochemistry 34*, 1295−1307.
31. Schurter, E. J., Yeh, H. J. C., Sayer, J. M., Lakshman, M. K., Yagi, H., Jerina, D. M., and Gorenstein, D. G. (1995) NMR solution structure of a nonanucleotide duplex with a dG mismatch opposite a 10*R* adduct derived from trans addition of a deoxyadenosine N^6-amino group to (−)-(*7S,8R,9R,10S*)-7,8-dihydroxy-9,10-epoxy-7,8,9,10-tetrahydrobenzo-[a]pyrene. *Biochemistry 34*, 1364−1375.
32. Yeh, H. J. C., Sayer, J. M., Liu, X., Altieri, A. S., Byrd, R. A., Lakshman, M. K., Yagi, H., Schurter, E. J., Gorenstein, D. G., and Jerina, D. M. (1995) NMR solution structure of a nonanucleotide duplex with a dG mismatch opposite a 10*S* adduct derived from trans addition of a deoxyadenosine N^6-amino group to (+)-(7*R*,8*S*,9*S*,10*R*)-7,8-dihydroxy-9,10-epoxy-7,8,9,10-tetrahydrobenzo[a]pyrene: an unusual syn glycosidic torsion angle at the modified dA. *Biochemistry 34*, 13570−13581.
33. Zegar, I. S., Kim, S. J., Johansen, T. N., Harris, C. M., Harris, T. M., and Stone, M. P. (1996) Adduction of the human *N-ras* codon 61 sequence with (−)-(7*S*,8*R*,9*R*,10*S*)-7,8-dihydroxy-9,10-epoxy-7,8,9,10-tetrahydrobenzo[a]pyrene: structural refinement of the intercalated *SRSR* (61,2) (−)-7*S*,8*R*,9*S*,10*R*)-N^6-[10-(7,8,9,10-tetrahydrobenzo[a]pyrenyl]-2′-deoxyadenosyl adduct from ^{1}H NMR. *Biochemistry 35*, 6212−6224.
34. Altona, C., and Sundaralingam, M. (1972) Conformational analysis of the sugar ring in nucleosides and nucleotides. A new description using the concept of pseudorotation. *J. Am. Chem. Soc. 94*, 8205−8212.
35. Pearlman, D., Case, D., Caldwell, J., Seibel, G., Singh, U. C., Weiner, P., and Kollman, P. A. (1986) AMBER 4.0 Documentation, Copyright 1986, 1991, University of California.
36. Hingerty, B. E., Ritchie, R. H., Ferrell, T. L., and Turner, J. E. (1985) Dielectric effects in biopolymers: the theory of ionic saturation revisited. *Biopolymers 24*, 427−439.
37. Friedman, R. A., and Honig, B. (1992) The electrostatic contribution to DNA base stacking interactions. *Biopolymers 32*, 145−159.
38. Atkins, P. W. (1990) *Physical Chemistry*, 4th Ed., pp 661−662, W. H. Freeman Co, New York.
39. Berman, H. M. (1997) Crystal studies of B-DNA: the answers and the questions. *Biopolymers* (Nucleic Acid Sciences) *44*, 23−44.
40. Olson, W. K. (1973) *Syn-anti* effects on the spatial configuration of polynucleotides. *Biopolymers 12*, 1787−1814.
41. Sundaralingam, M. (1973) The concept of a conformationally "rigid" nucleotide and its significance in polynucleotide conformational analysis in conformations of biological molecules and polymers. *Jerusalem Symposia on Quantum Chemistry and Biochemistry* (Bergmann, E. D., and Pullman, B., Eds.) pp 417−456, Academic Press, New York.
42. Xie X. (1998) Origin of opposite orientations in stereoisomeric DNA guanine adducts derived from benzo[a]pyrene diol epoxides with different tumorigenic potentials: a computational study of modified nucleosides. Ph.D. Thesis, NYU.
43. Feng, B., Gorin, A., Hingerty, B. E., Geacintov, N. E., Broyde, S., and Patel, D. J. (1997) Structural alignment of the (+)-*trans-anti*-benzo[a]pyrene-dG adduct positioned opposite dC at a DNA template-primer junction. *Biochemistry 36*, 13769−13779.
44. Cosman, M., Hingerty, B. E., Geacintov, N. E., Broyde, S., and Patel, D. J. (1995) Structural alignments of (+) and (−)-*trans-anti*-benzo[a]pyrene-dG adducts positioned at a DNA replication fork. *Biochemistry 34*, 15334−15350.
45. Mao, B., Hingerty, B. E., Broyde, S., and Patel D. J. (1998) Solution Structure of the aminofluorene [AF]-intercalated conformer of the syn [AF]-C8-dG adduct opposite dC in a DNA duplex. *Biochemistry 37*, 81−94.
46. Mao, B., Hingerty, B. E., Broyde, S., and Patel, D. J. (1998) Solution Structure of the aminofluorene [AF]-external conformer of the anti [AF]-C8-dG adduct opposite dC in a DNA duplex. *Biochemistry 37*, 95−106.
47. Patel D., Mao, B., Gu, Z., Hingerty, B. E., Gorin, A., Basu, A.; Broyde, S. (1998) NMR solution structures of covalent aromatic amine-DNA adducts and their mutational relevance. *Chem. Res. Toxicol. 11*, 391−407.
48. Rodriguez, H.; Loechler, E. L. (1993) Mutational specificity of the (+)-*anti*-diol epoxide of benzo[a]pyrene in a supF gene of an *Escherichia coli* plasmid: DNA sequence context influences hotspots, mutagenic specificity and the extent of SOS enhancement of mutagenesis. *Carcinogenesis 14*, 373−383.
49. Rodriguez, H., and Loechler, E. L. (1993) Mutagenesis by the (+)-*anti*-diol epoxide of benzo[a]pyrene: what controls mutagenic specificity? *Biochemistry 32*, 1759−1769.
50. Rodriguez, H., and Loechler, E. L. (1995) Are base substitution and frameshift mutagenesis pathways interrelated? An analysis based upon studies of the frequencies and specificities of mutations induced by the (+)-*anti*-diol epoxide of benzo[a]-pyrene. *Mutat. Res. 326*, 29−37.
51. Moriya, M., Spiegel, S., Fernandes, A., Amin, S., Liu, T., Geacintov, N., and Grollman, A. P. (1996) Fidelity of translesional synthesis past benzo[a]pyrene diol epoxide-2′-deoxyguanosine DNA adducts: marked effects of host cell, sequence context, and chirality. *Biochemistry 35*, 16646−16651.
52. Shukla, R., Liu, T., Geacintov, N. E., and Loechler, E. L. (1997) The major, N^2-dG adduct of (+)-*anti*-B[a]PDE shows a dramatically different mutagenic specificity (predominantly, G → A) in a 5′-CGT-3′ sequence context. *Biochemistry 36*, 10256−10261.
53. Shukla, R., Jelinsky, S., Liu, T., Geacintov, N. E., and Loechler E. L. (1997) How stereochemistry affects mutagenesis by N^2-deoxyguanosine adducts of 7,8-dihydroxy-9,10-epoxy-7,8,9,-10-tetrahydrobenzo[a]pyrene: configuration of the adduct bond is more important than those of the hydroxyl groups. *Biochemistry 36*, 13263−13269.
54. Fernandes, A., Liu, T., Amin, S., Geacintov, N. E., Grollman, A. P., and Moriya, M. (1998) Mutagenic potential of stereoisomeric bay region (+) and (−)-*cis-anti*-benzo[a]pyrene diol epoxide-N^2-2′-deoxyguanosine adducts in *Escherichia coli* and simian kidney cells. *Biochemistry 37*, 10164−10172.
55. Page J. E., Zajc, B., Oh-hara, T., Lakshman, M. K., Sayer, J. M., Jerina, D. M., and Dipple, A. (1998) Sequence context profoundly influences the mutagenic potency of trans-opened benzo[a]pyrene 7,8-diol-epoxide-purine nucleoside adducts in site-specific mutation studies. *Biochemistry 37*, 9127−9137.

56. Xu, R., Mao, B., Amin, S., and Geacintov, N. E. (1998) Bending and circularization of site-specific and stereoisomeric carcinogen-DNA adducts. *Biochemistry 37*, 769−778.
57. Kozack, R., and Loechler, E. L., (1997) Molecular modeling of the conformational complexity of (+)-*anti*-B[a]PDE-adducted DNA using simulated annealing. *Carcinogenesis 18*, 1585−1593.
58. Kozack, R., and Loechler, E. L. (1999) Molecular modeling of the major adduct of (+)-*anti*-B[a]PDE (N2-dG) in the eight conformations and five DNA sequences most relevant to base substitution mutagenesis. *Carcinogenesis 20*, 85−94.
59. Kozack, R., and Loechler E. L. (1999) A hypothesis for what conformation of the major adduct of (+)-*anti*-B[a]PDE (N^2-dG) causes G→T vs G→A mutations based upon a correlation between mutagenesis and molecular modeling results. *Carcinogenesis 20*, 95−102.
60. Mao, B., Li, B., Amin, S., Cosman, M., and Geacintov, N. E. (1993) Opposite stereoselective resistance to digestion by phosphodiesterases I and II of benzo[a]pyrene diol epoxide-modified oligonucleotide adducts. *Biochemistry 32*, 11785−11793.
61. Broyde S., and Hingerty B. E. (1984) Mutagenicity of polycyclic aromatic hydrocarbons and amines: a conformational hypothesis. *Ann. N.Y. Acad. Sci. 435*, 119−122.

BI9825605